JOURNAL OF Materials CHEMISTRY

Characterization of $Ce_3(SiS_4)_2I$, a compound with a new structure type

Gilles Gauthier,[a] Shinji Kawasaki,[a] Stéphane Jobic,[a] Pierre Macaudière,[b] Raymond Brec*[a] and Jean Rouxel[a]

[a]*Institut des Matériaux de Nantes, BP 32229, 44322 Nantes Cedex 03, France*
[b]*Centre de Recherches de Rhône-Poulenc, 52 rue de la Haie Coq, 93308 Aubervilliers Cedex, France*

The first cerium iodothiosilicate, $Ce_3(SiS_4)_2I$, has been synthesized from the reaction of cerium sulfide with silicon, iodine and sulfur at high temperature. This compound crystallizes in the monoclinic symmetry (space group $C2/c$ and $Z=4$) with the powder refined cell parameters: $a=15.9634(5)$, $b=7.8502(2)$, $c=10.8664(3)$ Å, $\beta=97.931(2)°$. The crystal structure was refined to $R(\%)=2.17$ and $R_w(\%)=2.60$ from single crystal X-ray diffraction data. $Ce_3(SiS_4)_2I$ presents tunnels in which are located the iodide anions surrounded by three ceriums, in $[ICe_3]$ isosceles triangular entities. The tunnels are constituted of a three dimensional network made of $(CeIS_8)$ polyhedra (trigonal prisms of sulfur tricapped by two sulfur and one iodine atom) linked to (SiS_4) tetrahedra. Magnetic susceptibility measurements and UV–VIS diffuse reflectance spectroscopy are consistent with the occurrence of Ce^{III} ions, whereas band structure calculations indicate that the phase is a semiconductor. The charge balance in the material can be written as : $Ce^{III}{}_3Si^{IV}{}_2I^{-I}S^{-II}{}_8$.

Rare-earth (RE) chalcogenides present a rich structural chemistry[1–3] and widely varying physical properties[4–7] related to a common high coordination of the RE elements and the occurrence of unsaturated f-subshells. With low spatial extension of the f orbitals associated with localized energy levels, one observes high magnetic moments (for elements such as Tb, Dy, Ho and Er), narrow band emission and absorption spectra, *etc*. These interesting magnetic and optical properties led to the use of the RE chalcogenides as phosphors,[4–5] magneticooptical[6] and optical window[7] materials. Some of these phases have also been used more recently as industrial pigments.[5]

For the last 20 years, research on quaternary compounds has extensively developed with the synthesis of new chalcogenides containing an alkali or alkaline earth metal, a lanthanide, and a main group metal or a transition metal.[8] This intense activity in RE solid state chemistry is in part related to the discovery of high temperature superconducting cuprates containing an RE element and to the attempts to extend the superconducting properties from oxides to chalcogenides. In addition, this development has been favored by the ability of the (A_2Q_x) reactive flux method (A = alkali metal or alkaline earth metal, Q = chalcogen) to stabilize metastable structures in ternary and quaternary compounds. This novel synthesis route, initially developed for new transition or main group element chalcogenide preparations,[9] has been successfully extended to RE elements yielding new materials with original structures, new stoichiometries and properties.[10]

For all the above reasons, we have tried to prepare new phases in the RE–A–X–Q (A = group 14 element, X = halogen and Q = chalcogen) system. We thus report the synthesis and the characterization of the first iodothiosilicate of cerium.

Experimental

Synthesis

$Ce_3(SiS_4)_2I$ was prepared from silicon (88.4 mg, 3.15 mmol, Koch-Light Laboratories, 99.99%), sulfur (185.2 mg, 5.775 mmol, Fluka, puriss. > 99.999%), iodine (133.2 mg, 0.525 mmol, Aldrich chem., 99.99 + %), and Ce_2S_3 (593 mg, 1.575 mmol Cerac, −325 mesh powder, 99.9%), taken in the ratio Ce : Si : I : S = 3 : 3 : 1 : 10 [$Ce_3(SiS_4)_2I : SiS_2 = 1 : 1$]. The starting materials were placed in an evacuated (10^{-3} Torr) quartz tube, sealed and heated at 700 °C for 4 d. The sample was then slowly cooled to room temperature, finely ground and fired to 900 °C under the same conditions. This two step reaction yielded pure well crystallized and air-stable $Ce_3(SiS_4)_2I$ as the SiS_2 excess condensed at the coldest end of the reaction tube. From the powder, crystals were separated out for a crystallographic analysis. A microprobe analysis by energy dispersive X-ray spectroscopy (EDXS) performed with a JEOL 5800-LV SEM instrument equipped with a PGT IMIX detector gave the chemical formula $Ce_3Si_{2.1}I_{0.9}S_{7.8}$ in satisfactory agreement with the stoichiometry $Ce_3(SiS_4)_2I$ found from the structural determination (see below).

X-Ray structure determination

A well shaped yellowish transparent crystal (0.17 × 0.06 × 0.03 mm) was selected and mounted on a STOE Image Plate X-ray diffractometer for room temperature data collection. A series of diffraction patterns was recorded by rotating an unorientated crystal in the X-ray beam. Images were recorded over a 249.2° ϕ range with a 1.4° increment angle. Indexing was performed using the program INDEX.[11] Cell parameters were determined from a least squares analysis of the setting angles of 4876 reflections in the range $2.9 \leqslant 2\theta/\text{degrees} \leqslant 48.4$. Accurate cell constants [$a=15.9634(5)$, $b=7.8502(2)$, $c=10.8664(3)$ Å, $\beta=97.931(2)°$] were extracted from a full pattern matching refinement (FULLPROF[12]) from a powder diagram recorded on a CPS 120 INEL X-ray powder diffractometer using monochromatized Cu-K-L_2 radiation and equipped with a position-sensitive detector calibrated with $Na_2Ca_3Al_{12}F_{14}$ as standard. The powder was sieved at 20 μm and introduced into a Lindemann capillary (id = 0.1 mm). The diagram reflections could all be satisfactorily indexed and the ensuing parameter refinement left no lines unaccounted for, indicating a good purity of the sample, at the X-ray diffraction detection threshold. The *hkl* interreticular distances with observed intensities are gathered in Table 1.

Table 1 X-Ray powder diffraction pattern of $Ce_3(SiS_4)_2I$: d_{hkl} spacing and observed intensities for main reflections (full pattern matching refinement: $R_p = 3.37\%$; $R_{wp} = 4.41\%$; $R_{exp} = 3.61\%$; $\chi^2 = 1.49$; $R_{Bragg} = 1.72\%$)[12]

h	k	l	d_{hkl}/Å	I_{obs}	h	k	l	d_{hk}/Å	I_{obs}
2	0	0	7.905	3.93	0	2	4	2.2192	6.78
1	1	0	7.031	2.34	2	2	−4	2.2029	6.39
1	1	−1	6.059	17.47	6	2	−1	2.1935	5.06
1	1	1	5.728	4.32	6	2	0	2.1878	9.26
0	0	2	5.381	100.00	7	1	−1	2.1846	7.74
3	1	0	4.376	6.09	7	1	0	2.1706	10.76
3	1	−1	4.226	17.72	1	3	−3	2.1182	16.96
2	0	2	4.188	38.24	6	2	−2	2.1129	4.53
1	1	2	4.152	36.56	3	3	2	2.1020	13.24
4	0	0	3.9526	18.13	6	2	1	2.0975	18.34
0	2	0	3.9250	23.88	1	1	−5	2.0945	3.38
3	1	1	3.9005	38.40	4	0	4	2.0939	2.92
0	2	1	3.6875	73.02	1	3	3	2.0734	5.52
2	2	0	3.5156	6.02	7	1	−3	1.9768	3.77
4	0	−2	3.4186	52.22	6	2	−3	1.9709	3.65
2	2	−1	3.4040	13.51	0	4	0	1.9625	6.02
2	2	1	3.2829	6.69	5	3	1	1.9507	4.02
1	1	−3	3.2780	9.26	8	0	−2	1.9440	4.96
3	1	2	3.2192	9.95	3	3	3	1.9092	11.58
0	2	2	3.1711	7.03	2	4	0	1.9047	6.48
2	2	−2	3.0295	47.80	1	3	−4	1.8841	12.78
4	0	2	2.9946	6.09	2	4	1	1.8649	10.57
5	1	0	2.9331	30.27	5	1	−5	1.8521	6.14
2	2	2	2.8638	9.35	3	3	−4	1.8235	3.75
4	2	0	2.7851	21.70	2	4	−2	1.8146	5.35
4	2	−1	2.7622	90.05	2	0	−6	1.8038	4.41
5	1	1	2.7422	20.59	4	2	−5	1.7894	7.45
5	1	−2	2.7261	15.51	2	2	5	1.7875	15.77
0	0	4	2.6906	3.81	6	2	3	1.7794	10.04
2	0	−4	2.6616	13.54	2	4	2	1.7771	5.24
0	2	3	2.6480	35.39	8	2	0	1.7652	3.61
6	0	0	2.6351	23.37	1	1	−6	1.7642	6.83
4	2	1	2.6349	18.32	4	4	−1	1.7520	4.07
3	1	3	2.6304	27.51	9	1	−1	1.7295	3.79
2	2	−3	2.5917	8.66	4	0	−6	1.7255	7.52
1	3	0	2.5816	8.30	3	3	4	1.7159	3.86
4	2	−2	2.5779	8.99	9	1	0	1.7143	4.18
1	1	−4	2.5660	37.74	7	3	0	1.7098	4.89
1	3	−1	2.5233	3.65	8	2	1	1.7086	5.72
6	0	−2	2.5071	10.39	2	0	6	1.6994	11.28
1	3	1	2.4976	5.29	7	3	−2	1.6810	15.03
1	1	4	2.4630	18.55	1	3	−5	1.6718	5.91
2	0	4	2.4462	20.80	9	1	1	1.6586	6.30
2	2	3	2.4373	25.67	5	1	5	1.6382	4.39
4	0	−4	2.3823	20.78	3	3	−5	1.6361	4.89
4	2	2	2.3808	22.94	4	4	−3	1.6182	7.10
1	3	−2	2.3483	7.01	7	3	−3	1.6102	11.81
3	3	0	2.3437	27.17	6	2	4	1.6096	9.10
3	3	−1	2.3198	11.63	7	1	4	1.5895	5.77
4	2	−3	2.3115	42.50	7	3	2	1.5825	4.55
3	3	1	2.2614	34.61	10	0	−2	1.5769	10.32
6	0	2	2.2473	26.36	8	2	−4	1.5671	7.63

Concerning monocrystal data collection, the reflections were recorded in the $-18 \leqslant h \leqslant 18$, $-8 \leqslant k \leqslant 8$, and $-11 \leqslant l \leqslant 11$ space. After the Lorentz polarization reduction of the 10692 raw data, a set of 4032 reflections with $I \geqslant 3\sigma(I)$ was kept for data refinement. The structure was solved using the direct method of the SHELXTL program[13] followed by successive observed and difference Fourier syntheses calculated with the JANA96[14] structure determination package. Conventional atomic and anomalous scattering factors were taken from the usual sources.

The diffraction data analysis indicated a $2/m$ Laue symmetry with limiting conditions consistent with the $C2/m$ space group. After averaging (853 independent reflections, $R_{int} = 4.55\%$), the first refinement cycle series with isotropic atomic displacement parameter (ADP) yielded a satisfactory R value of 5.32%. Anisotropic ADPs and an isotropic secondary extinction parameters (66 variables in all) led to $R_F = 2.17\%$, $R_{wF} = 2.60\%$. The final difference electron density showed features no higher than $0.89\ e^-\ Å^{-3}$ and no lower than $-1.85\ e^-\ Å^{-3}$. The crystal data and the recording conditions of the structural study are summarized in Table 2. The atomic parameters and anisotropic thermal parameters are gathered in Table 3 and Table 4. Bond distances and angles of the phase constituting polyhedra are given in Table 5.

Physical property measurements

The variable temperature magnetic data were recorded on a Quantum Design MPMS-5 SQUID magnetometer in a field of 1000 G. The sample powder was loaded into a 3 mm diameter Suprasyl® (Heraeus) silica tube in a glovebox. A 1 cm long silica piston was used to maintain the powder in the tube bottom. All magnetic susceptibility data were corrected for core diamagnetism ($\chi_{dia} = -4.0294.10^{-4}$).[15]

The room temperature UV–VIS–NIR diffuse reflectance spectrum was recorded with a Perkin Elmer Lambda II spectrometer. This instrument was equipped with a 60 mm diameter integrating sphere and computer controlled using the PECOL software. The reflectance *vs.* wavelength measurements were made in the range 210–1100 nm (*i.e.* from *ca.* 1.1 to 5.9 eV) using $BaSO_4$ powder (Perkin Elmer Standard) as reference (100% reflectance).

Self-consistent *ab initio* band structure calculations were performed using the TB–LMTO–ASA (tight-binding linear muffin-tin orbital in the atomic sphere approximation) method in its scalar relativistic version.[16–18] All reciprocal space integrations were performed with the tetrahedron method[19] using 32 irreducible k-points within the Brillouin zone. The basis sets consisted of 6s, 5f and 4d orbitals for Ce, 3s and 3p for Si, 5p for I, and 3s and 3p for S. The 6p orbitals for Ce, 3d for Si, 6s, 5d and 5f for I, and 3d for S were treated with the downfolding technique. To achieve space filling within the atomic sphere approximation, interstitial spheres were introduced to avoid too large overlaps of the atom centered spheres. The sixteen empty sphere positions and optimum sphere radii were calculated using an automatic procedure developed by Krier *et al.*[20] We did not allow overlaps >15% for any two atom centered spheres.

Results and Discussion

Structure of $Ce_3(SiS_4)_2I$

The tridimensional structure of $Ce_3(SiS_4)_2I$ is based on a $Ce_3(SiS_4)_2$ skeleton defining tunnels filled by iodide. A general view of the structure along the ***c*** axis is given in Fig. 1. Because of the well known stability of Ce^{III} ($4f^1$) in chalcogenides, the $Ce^{III}{}_3(Si^{IV}S^{-II}{}_4)_2I^{-I}$ charge balance can be *a priori* proposed. Ce(1) and Ce(2) first coordination spheres are similar. The two cerium atoms are surrounded by eight S^{-II} and one I^- anions in (CeS_8I) polyhedra that can be considered as (CeS_6) triangular prisms [see Fig. 2(*a*)] capped by two chalcogens and one halogen located roughly on a perpendicular to the rectangular faces. It is noticed that some of the Ce—S distances involving capping sulfur atoms are much smaller than those of the (CeS_6) prism [for example Ce(2)—S(4) 2.904(2) Å *vs.* Ce(2)—S(3) 3.285(2) Å]. The mean Ce—S distances [Ce(1)—S 3.007(2) Å, Ce(2)—S 3.096(2) Å] are in accord with those found in the literature [from 2.901(2) to 3.092(2) Å in γ-Ce_2S_3 for instance].[21] They correspond well to the sum of the ionic radii [$d(Ce^{III}-S^{-II} = 3.036$ Å].[22] The smallest contact distance between sulfur ions [S(3)···S(3) 3.298(2) Å], a little shorter than that usually observed (*ca.* 3.46 Å in TiS_2 for example),[23] can be attributed to steric effects, in relation with the high degree of coordination of the Ce^{III} cations. Nevertheless, it remains sufficiently large to exclude any sulfur–

Table 2 Crystallographic data and experimental details for $Ce_3(SiS_4)_2I$

physical and crystallographic data
formula: $Ce_3(SiS_4)_2I$, molar mass: 859.917
color: yellowish, crystal size/mm^3: $0.17 \times 0.06 \times 0.03$
system: monoclinic, space group: $C2/c$ (no. 15)
cell parameters (powder refinement, $T = 300$ K):
$a = 15.9634(5)$, $b = 7.8502(2)$, $c = 10.8664(3)$ Å, $\beta = 97.931(2)°$
$V = 1348.7(1)$ Å^3, $Z = 4$, $D_c = 4.201$ g cm^{-3}
absorption coefficient $\mu(\lambda_{Mo\text{-}K\text{-}L2,3}) = 137$ cm^{-1}
recording conditions
temperature: 300 K, radiation: $\lambda_{MoK\text{-}L2,3} = 0.71069$ Å, diffractometer: STOE image plate
angular range $2\theta/°$: 2.9–48.4, hkl range: $-18 \leqslant h \leqslant 18, +8 \leqslant k \leqslant 8, -11 \leqslant l \leqslant 11$
data reduction
total recorded reflections: 10692, observed reflections [$I > 3\sigma(I)$]: 4032
independent reflections [$I > 3\sigma(I)$]: 853, $R_{int}(\%) = 4.55$
refinement
weighting scheme: $w = 1/(\sigma^2|F_o| + (0.01 \times 1.5|F_o|)^2)$
no. of refined parameters: 66
refinement results: $R(\%) = 2.17$, $R_w(\%) = 2.60$, GOF = 0.87
secondary extinction coefficient: 0.119(6), type: isotropic, type I, Gaussian distribution
residual electronic density: -1.85, $+0.89$ e$^-$ Å^{-3}

sulfur bonding interactions. The same occurs in $CePS_4$ for which a very short S···S distance of 3.035 Å is observed.[24]

The shortest non-bonding S···S contacts have been found in PV_2S_{10}[25] and $V(S_2C_2Ph_2)_3$ [26] with interligand S···S contact distances of 2.972 and 2.927 Å, respectively, in bicapped VS_8 prisms. Electronic band structure calculations carried out on both compounds[27] have shown slightly negative overlap populations for these very short contacts, ruling out any sulfur–sulfur bonding interaction. These short contacts occur largely because the cation is small in size so that the ligands coordinating around each metal cation are squeezed to one another. According to these results, use of a larger metal cation should lead to longer interligand S···S contacts. With a cationic radius of Ce^{III} of 1.20 Å as compared to 0.73 Å for V^{IV}, a somewhat longer distance is expected for the latter cation compounds. This is what is observed in the present case.

I^- is coordinated by three cerium cations to form isosceles ICe_3 triangles, as shown in Fig. 2(*b*). Within these groups, the Ce—I distances [Ce(2)—I 3.2954(9) Å, Ce(1)—I 3.4324(4) Å (×2)] agree with those observed for example in CeSI [from 3.301(1) to 3.4368(4)].[28] Again, these values compare satisfactorily with the sum of the ionic radii [$d(Ce^{III}-I^-) = 3.396$ Å].[22] In the structure tunnels, two successive Ce_3I triangles, 5.4390(2) Å apart along ***c***, define empty iodine-two-face-centered Ce_6I_2 octahedra. Concerning the iodide anisotropic ADP,

Table 3 Fractional atomic coordinates and equivalent isotropic atomic displacement parameters of $Ce_3(SiS_4)_2I$

atom	x	y	z	U_{eq}/Å^2
Ce(1)	0.19688(2)	0.12029(5)	0.68020(4)	0.0093(2)
Ce(2)	1/2	0.09620(7)	3/4	0.0114(2)
I	0	0.98401(8)	1/4	0.0211(3)
Si	0.1596(1)	0.4628(2)	0.0292(2)	0.0097(6)
S(1)	0.1446(1)	0.2557(2)	0.1463(2)	0.0119(6)
S(2)	0.28161(9)	0.5690(2)	0.0857(2)	0.0111(5)
S(3)	0.0682(1)	0.6538(2)	0.0426(2)	0.0117(6)
S(4)	0.1501(1)	0.3994(2)	−0.1605(2)	0.0111(6)

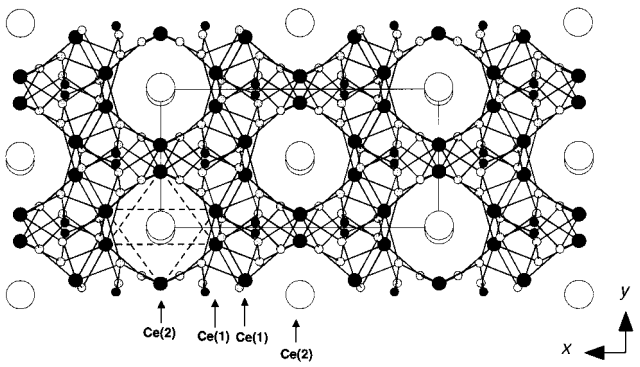

Fig. 1 View of $Ce_3(SiS_4)_2I$ down the ***c*** axis. Black atoms are Si, dark gray are Ce, light gray are S and white are I.

Table 5 Bond distances (Å) and angles (°) in $Ce_3(SiS_4)_2I$ polyhedra

[Ce(1)S_8I] group			[SiS_4] group		
Ce(1)—S(1)	3.096(2)		Si—S(1)	2.099(3)	
Ce(1)—S(1)	3.075(2)		Si—S(2)	2.130(2)	
Ce(1)—S(2)	2.925(2)		Si—S(3)	2.111(3)	
Ce(1)—S(2)	2.983(2)		Si—S(4)	2.106(3)	
Ce(1)—S(2)	3.036(2)				
Ce(1)—S(3)	2.958(2)				
Ce(1)—S(4)	2.952(2)				
Ce(1)—S(4)	3.027(2)				
Ce(1)—I	3.4324(4)				
[Ce(2)S_8I] group			[ICe_3] group		
Ce(2)—S(1)	2.945(2)	(×2)	I—Ce(1)	3.4324(4)	(×2)
Ce(2)—S(3)	3.248(2)	(×2)	I—Ce(2)	3.2954(9)	
Ce(2)—S(3)	3.285(2)	(×2)	Ce(1)—I—Ce(2)	103.80(1)	(×2)
Ce(2)—S(4)	2.904(2)	(×2)	Ce(1)—I—Ce(1)	152.40(2)	
Ce(2)—I	3.2954(9)				

Table 4 Anisotropic atomic displacement parameters of $Ce_3(SiS_4)_2I$

atom	U_{11}	U_{22}	U_{33}	U_{12}	U_{13}	U_{23}
Ce(1)	0.0083(2)	0.0116(3)	0.0081(3)	0.0012(1)	0.0015(2)	0.0007(1)
Ce(2)	0.0055(3)	0.0146(3)	0.0141(4)	0	0.0020(2)	0
I	0.0107(3)	0.0150(4)	0.0396(5)	0	0.105(3)	0
Si	0.0070(8)	0.012(1)	0.011(1)	0.0005(7)	0.0017(7)	0.0014(8)
S(1)	0.0095(8)	0.0125(9)	0.014(1)	0.0012(6)	0.0039(6)	0.0028(7)
S(2)	0.0071(7)	0.0152(9)	0.011(1)	−0.0019(7)	0.0007(6)	0.0010(7)
S(3)	0.0075(8)	0.0125(9)	0.015(1)	0.0002(6)	−0.0000(7)	−0.0020(7)
S(4)	0.0095(8)	0.0142(9)	0.010(1)	0.0013(6)	0.0012(6)	−0.0015(7)

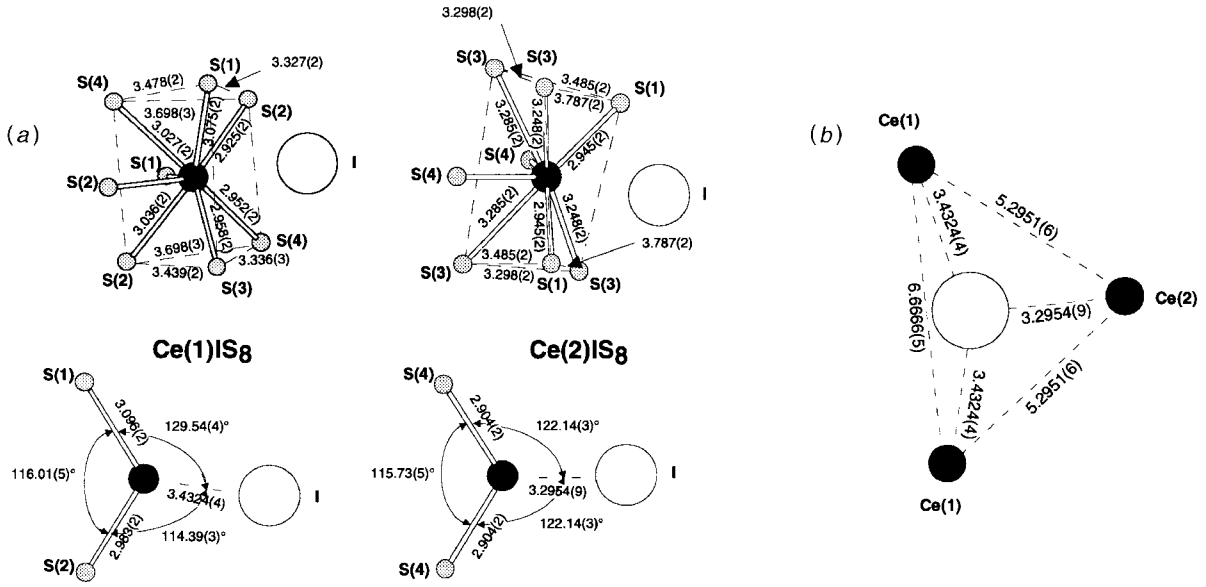

Fig. 2 (*a*) Anionic environment of the two kinds of cerium atoms in $Ce_3(SiS_4)_2I$. Dark gray atoms are Ce, light gray are S and white are I. (*b*) Planar triangular environment of iodide anions, showing $(ICe_3)^{8+}$ entities. Dark gray atoms are Ce and white is I.

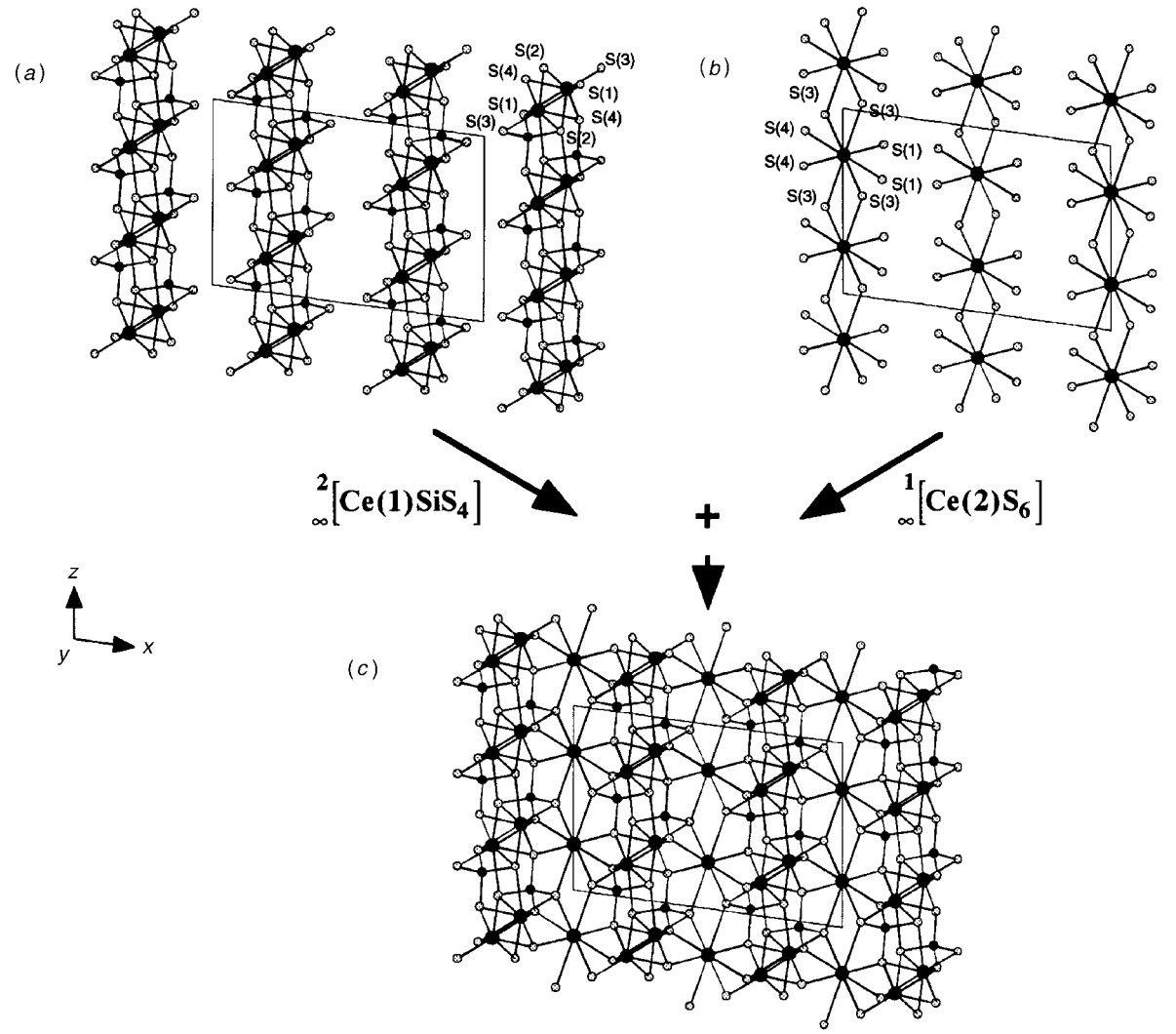

Fig. 3 Description of the $Ce_3(SiS_4)_2I$ structure: (*a*) view down the ***b*** axis showing the $_{\infty}{}^{2}[Ce(1)SiS_4]$ layers only; (*b*) same view down the ***b*** axis showing the $_{\infty}{}^{1}[Ce(2)S_6]$ ribbons only; (*c*) total view down the ***b*** axis. Black atoms are Si, dark gray are Ce, light gray are S. I are not shown for clarity.

it is noteworthy that its U_{33} parameter is almost three times higher than that of U_{11} and U_{22}. In spite of this elevated U_{33} value and because of the inter-iodide distance, anionic conductivity inside the tunnel is not expected.

Silicon cations are in tetrahedral sites, with the Si—S bonds and S—Si—S angles of the SiS_4 groups ranging from 2.099(3) to 2.130(2) Å, and from 106.2(1) to 114.3(1)°, respectively. These values are close to those observed for example in $Na_4Si_4S_{10}$ ($2.025 \leqslant d_{Si-S} \leqslant 2.162$ Å and $108.07 \leqslant S-Si-S \leqslant 111.51°$).[29]

From a descriptive point of view, the structure can be thought of as made of $_\infty{}^2[Ce(1)SiS_4]$ layers lying in the (100) plane [Fig. 3(*a*)] linked to each other through $_\infty{}^1[Ce(2)S_6]$ ribbons running along the ***c*** axis and built on S(3)—S(3) edge sharing CeS_8 dodecahedra [Fig. 3(*b*)]. The resulting 3D structure displays tunnels (along ***c***) to be found in the interspace between two layers and two chains [Fig. 3(*c*) and 1].

The $_\infty{}^2[Ce(1)SiS_4]$ layers themselves are constituted [Fig. 4(*a*)] of $_\infty{}^1[Ce(1)S_5]$ zigzagging ribbons running along the ***b*** axis and built upon triangular face sharing CeS_8 dodecahedra. These chains are linked to one another along the ***c*** direction by S(2)—S(2) edge sharing [Fig. 4(*b*)]. The SiS_4 tetrahedra reinforce the cohesion in the layers by bridging the $_\infty{}^1[Ce(1)S_5]$ ribbons above and below the $_\infty{}^2[Ce(1)S_4]$ layers [Fig. 3(*a*) and 4(*c*)].

Magnetism

The temperature-dependent magnetic susceptibility of $Ce_3Si_2SiS_8$ over the range 2–300 K is shown in Fig. 5. Zero field cooling and field cooling results are similar and evidence the pure paramagnetic behavior of the compound. The plot of the molecular magnetic susceptibility *vs.* temperature reflects a Curie–Weiss behavior but the $1/\chi = f(T)$ curve deviates from a straight line in the high temperature range. Fitting the data to the expression $\chi = C/(T-\Theta) + \chi_0$, χ_0 being the temperature-independent paramagnetic susceptibility, yielded the following values: $C = 1.53(1)$ emu K mol^{-1}, $\Theta = -4.7(3)$ K, $\chi_0 = 0.002\,48(5)$emu mol^{-1}. The cerium observed magnetic moment calculated at 300 K from the following formula:

$$\mu_{\text{eff}}(300\text{ K}) = \left(\frac{3kT\chi}{n_{\text{Ce}^{\text{III}}}N\beta^2}\right)^{\frac{1}{2}}$$

(with N = Avogadro number, k = Boltzman constant, β = Bohr magneton, $n_{\text{Ce}^{\text{III}}}$ = cerium number per formula unit) gives $\mu_{\text{eff}} = 2.45(2)\,\mu_B$, a value consistent with the theoretical magnetic moment of the Ce^{III} ion, *i.e.* $2.54\,\mu_B$. Owing to the $Ce^{III}{}_3(Si^{IV}S^{-II}{}_4)_2I^{-I}$ charge balance, magnetic behavior should be explained based only on the f^1 configuration of the Ce^{III} cation, or more precisely on the $^2F_{5/2}$ ground state spectroscopic term. Actually, the reality is more complex since a phenomenological temperature-independent parameter is required to obtain a good fit of the $1/\chi$ *vs.* T curve. Such a deviation from the Curie–Weiss law was predicted and found in the case of neodymium compounds[30] by taking into account the crystal field Hamiltonian in the paramagnetic susceptibility calculations using the complete Van Vleck formula. In our case, the crystal field of the Ce^{III} cations has a very low symmetry implying that the number of Kramers doublets originating in the $^2F_{5/2}$ term is probably maximum, *i.e.* equal to 3. The same behavior was recently observed by Ibers and co-workers for two Ce^{III} compounds, $BaCeCuS_3$ and $BaCeCuSe_3$[31] and by Kanatzidis and co-workers for $K_2Cu_2CeS_4$.[32]

Optical properties

The optical properties of $Ce_3(SiS_4)_2I$ were examined through diffuse reflectance measurements. The obtained spectrum (reflectance *vs.* energy) is shown in Fig. 6. The presence of a large absorption band, whose maximum lies between 2.8 and 3 eV, confirms the insulating nature of the compound with a gap around these values and it explains the yellowish color of the compound. According to the results of numerous studies

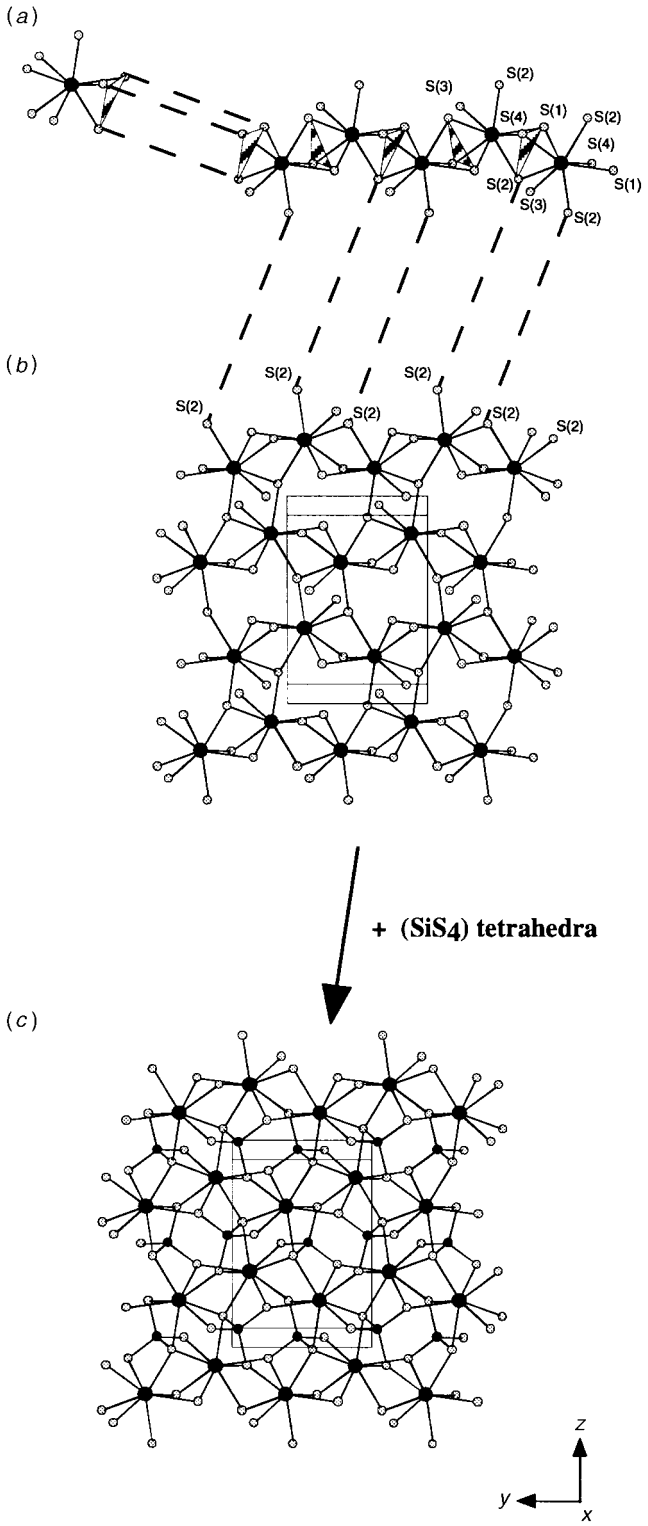

Fig. 4 Description of a $_\infty{}^2[Ce(1)SiS_4]$ layer along the ***a*** axis showing the $_\infty{}^1[Ce(1)S_5]$ ribbons: (*a*) building of one $_\infty{}^1[Ce(1)S_5]$ ribbon upon triangular face sharing (CeS_8) dodecahedra; (*b*) building of a $_\infty{}^2[Ce(1)S_4]$ layer from $_\infty{}^1[Ce(1)S_5]$ ribbons; (*c*) contribution of the (SiS_4) tetrahedra to build a $_\infty{}^2[Ce(1)SiS_4]$ layer. Black atoms are Si, dark gray are Ce, light gray are S. I are not shown for clarity.

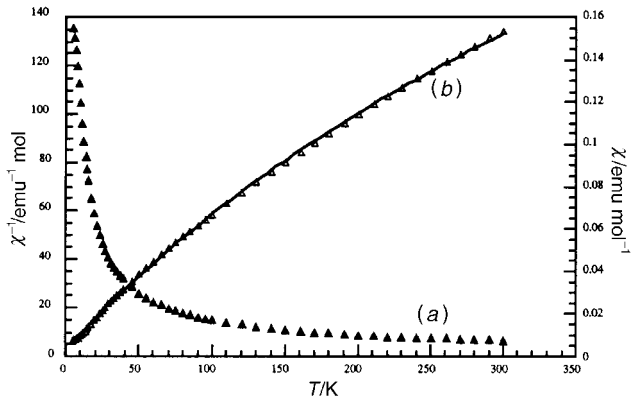

Fig. 5 Normal (*a*) and reciprocal (*b*) molar magnetic susceptibilities of $Ce_3(SiS_4)_2I$ as a function of temperature. The solid line is the result of fitting the data to the expression $\chi = C/(T-\Theta)+\chi_0$.

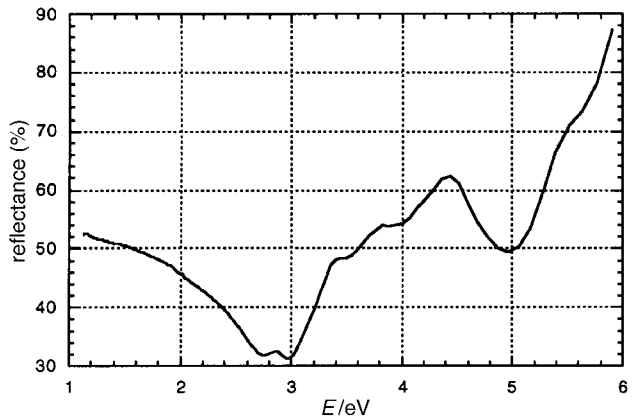

Fig. 6 Reflectance of $Ce_3(SiS_4)_2I$ as a function of energy

on γ-Ce_2S_3,[33] the transition which is responsible for this absorption can be attributed to the allowed electronic transfer from the narrow Ce $4f^1$ level to the conduction band, mainly built from the empty Ce 5d orbitals.

The compound exhibits also a second absorption band at *ca.* 5 eV, which can be attributed either to a transition from the Ce $4f^1$ level to higher levels in the conduction band, or, more likely, to a transition from the top of the valence band to the bottom of the conduction band (see below).

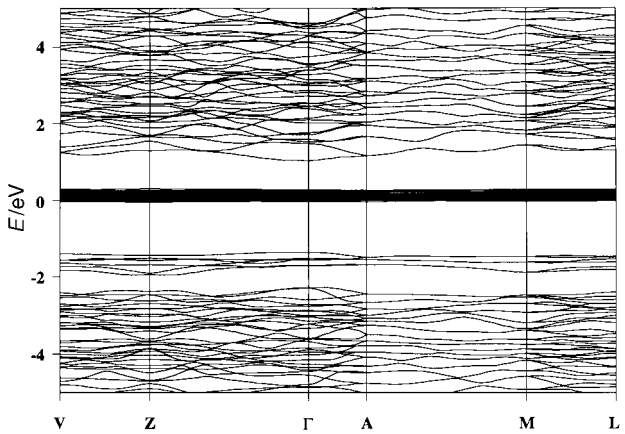

Fig. 8 Band structure of $Ce_3(SiS_4)_2I$ in the primitive reciprocal space[34]

Band structure calculations

Band structure calculations on $Ce_3(SiS_4)_2I$ have been performed in order to get some insight on the exact origin of the two absorption bands observed by diffuse reflectance.

The total density of states of $Ce_3(SiS_4)_2I$ in the $[-5,+5]$ eV energy range is provided in Fig. 7 with the atomic contributions of each element. The calculated band dispersion is shown in Fig. 8. The energy zero, taken at the Fermi level, lies within the Ce f block.

In the $[-5,+5]$ eV energy range, the DOS curve separates into three clearly defined regions of energy. The lower part (below -1.36 eV), that can be considered as an anionic sp band, constitutes the valence band (vb). Its uppermost non-bonding levels are based on iodine contribution [Fig. 7(*a*)] as expected from the anions electronegativity differences. The upper part of the diagram (above $+1.05$ eV) is a cation-based band, and is the so-called conduction band (cb). The cb bottom is built upon cerium d levels [Fig. 7(*b*)] while the Ce and Si

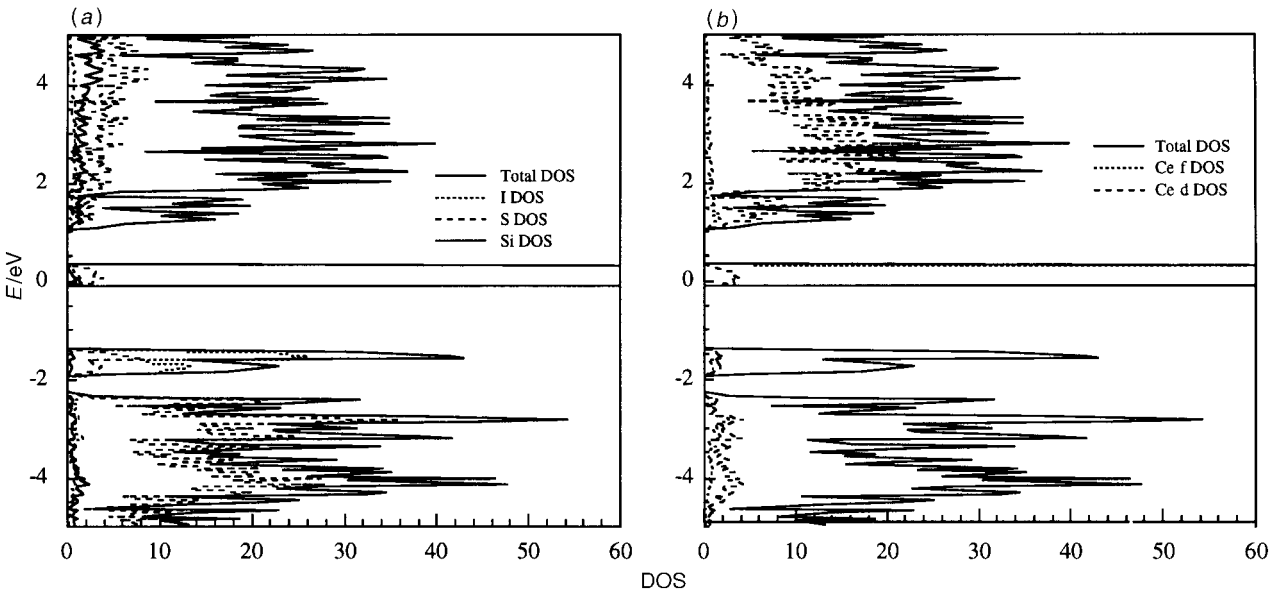

Fig. 7 Total density of states of $Ce_3(SiS_4)_2I$ with different atomic contributions

anti-bonding s and p levels are to be found at higher energy (not represented in Fig. 6). Between the vb and the cb, a fourteenth of the Ce f block is occupied. The non-dispersive character of the energy levels belonging to this block (Fig. 8) allows us to predict a semiconducting behavior for the phase. Moreover, the repulsion energy between Ce 4f orbital electrons, the so-called Hubbard *U* parameter, is estimated at about 6 eV[33c,35] preventing any f→f electron hopping conduction.

In contrast to its heavier lanthanide congeners for which absorption and emission phenomena take place in the visible range between numerous discrete levels corresponding to spectroscopic terms, Ce^{III} is characterized by only two spectroscopic terms, $^2F_{5/2}$ and $^2F_{7/2}$, separated by about 0.3 eV.[36] An $^2F_{5/2}$ to $^2F_{7/2}$ transition would induce an absorption in the IR region. Therefore, the position of the 5d levels at an energy lower than the excited Ce f^2 band, makes optical transitions very dependent on the chemical environment of cerium. For this reason, color may vary from pale yellow in the present compound to red in γ-Ce_2S_3, and has to be explained in terms of atomic-like f→d transitions. In $Ce_3(SiS_4)_2I$, the energy gap associated with this absorption threshold is estimated at 1.05 eV by the TB–LMTO–ASA method. Such a value appears quite small compared with the expected value of *ca.* 2.7 eV observed by diffuse reflectance. This discrepancy originates not only in the TB–LMTO–ASA method itself, well known to underestimate the energy gap, but also in the difficulty of taking into account the localized f levels in this type of calculation. Gap energies deduced from our calculations have then to be considered more qualitatively than quantitatively. In a similar way, the calculated vb→cb gap of 2.53 eV (Fig. 7) may be related to the 5 eV UV absorption threshold observed by reflectance, no significant inflection in the conduction band density of states being observed.

Conclusion

A compound with a new structure type, $Ce_3(SiS_4)_2I$, has been found and some of its physical properties determined. Because the material presents stable and well known polyhedra with stable ion oxidation states, the game of substitutions can certainly be played on the phase's four constituent elements. Already three isotypical compounds could be obtained through substitution of I by Br and Cl, and S by Se.[37] This should indeed lead to some modifications in the f^1→cb transitions energy, modifications that are currently under study through band structure and optical property determinations.

The research has been made possible by a grant (CIFRE no. 260/96) from Rhône-Poulenc Chimie and the 'Association Nationale de la Recherche Technique'. S. K. and G. G. acknowledge the financial support of 'Région des Pays de Loire' and Rhône-Poulenc Chimie, respectively. We also thank Florent Boucher for his help in running the TB–LMTO–ASA program.

References

1 J. Flahaut and P. Laruelle, in *Progress in the Science and Technology of the Rare Earths*, ed. L. Eyring, Pergamon Press, Oxford, 1968, vol. 3, p. 149.
2 J. Flahaut, in *Progress in the Science and Technology of the Rare Earths*, ed. L. Eyring, Pergamon Press, Oxford, 1968, vol. 3, p. 209.
3 J. Flahaut, in *Handbook on the Physics and Chemistry of Rare Earths*, ed. K. A. Gschneidner Jr. and L. R. Eyrings, North-Holland Publishing Company, Amsterdam, New York, Oxford, 1979, vol. 4, p. 1.
4 (*a*) G. Blasse, *Mater. Chem. Phys.,* 1992, **31** 3; (*b*) T. E. Peters and J. A. Baglio, *J. Electrochem. Soc.,* 1972, **119**, 230; (*c*) R. Ibañez, A. Garcia, C. Fouassier and P. Hagenmüller, *J. Solid State Chem.,* 1984, **53**, 406.
5 P. Maestro and D. Huguenin, *J. Alloys Compd.,* 1995, **225**, 520.
6 (*a*) B. A. Kolesov and I. G. Vasilyeva, *Mater. Res. Bull.,* 1992, **27**, 775; (*b*) F. J. A. M. Greidanus and W. Bas Zeper, *Mater. Res. Bull.,* 1990, **15**, 31.
7 J. D. Carpenter and S. J. Hwu, *Inorg. Chem.,* 1995, **34**, 4647.
8 (*a*) P. Wu and J. A. Ibers, *J. Alloys Compd.,* 1995, **229**, 206; (*b*) M. A. Pell and J. A. Ibers, *Chem. Ber.,* 1997, **130**, 1.
9 (*a*) S. A. Sunshine, D. Kang and J. A. Ibers, *J. Am. Chem. Soc.,* 1987, **109**, 6202; (*b*) M. G. Kanatzidis and A. C. Sutorik, *Prog. Inorg. Chem.,* 1995, **43**, 151.
10 (*a*) A. C. Sutorik and M. G. Kanatzidis, *Angew. Chem., Int. Ed. Engl.*, 1992, **31**, 1594; (*b*) P. Wu and J. A. Ibers, *J. Solid State Chem.,* 1993, **107**, 347; (*c*) A. C. Sutorik and M. G. Kanatzidis, *J. Am. Chem. Soc.,* 1994, **116**, 7706; (*d*) A. C. Sutorik, J. Albritton-Thomas, C. R. Kannewurf and M. G. Kanatzidis, *J. Am. Chem. Soc.,* 1994, **116**, 7706; (*e*) C. K. Bucher and S. Hwu, *Inorg. Chem.,* 1994, **33**, 5831; (*f*) A. E. Christuk, P. Wu and J. A. Ibers, *J. Solid State Chem.,* 1994, **110**, 330; (*g*) P. Wu, A. E. Christuk and J. A. Ibers, *J. Solid State Chem.,* 1994, **110**, 337; (*h*) J. H. Chen and P. K. Dorhout, *Inorg. Chem.,* 1995, **34**, 5705; (*i*) J. D. Carpenter and S. Hwu, *Inorg. Chem.,* 1995, **34**, 4647; (*j*) J. H. Chen, P. K. Dorhout and J. E. Ostenson, *Inorg. Chem.,* 1996, **35**, 5627; (*k*) A. C. Sutorik and M. G. Kanatzidis, *Chem. Mater.,* 1997, **9**, 387.
11 STOE IPDS Software Manual, version 2.75, 1996.
12 J. Rodriguez-Carjaval, *Physica B,* 1993, **192**, 55.
13 G. M. Sheldrick, SHELXTL version 5, Siemens Analytical X-Ray Instruments, Inc. Madison, WI, 1994.
14 V. Petøíèek, M. Dusek, JANA'96 Crystallographic Computing System, Institute of Physics, Academy of Sciences of the Czech Republic, Prague.
15 (*a*) P. Pascal, *Ann. Chim. Phys.,* 1910, **19**, 5; 1912, **25**, 289 and subsequent papers; (*b*) W. Klemm, in *Magnetochemie,* Akademische Verlagsgesellschaft, Leipzig, 1936; (*c*) P. W. Selwood, in *Magnetochemistry,* Interscience Publishers, New York, 1956.
16 O. K. Andersen, *Phys. Rev. B*, 1975, **12**, 3060.
17 O. K. Andersen and O. Jepsen, *Phys. Rev. Lett.,* 1984, **53**, 2571.
18 O. Jepsen and O. K. Andersen, *Z. Phys. B,* 1995, **97**, 35.
19 O. Jepsen, O. K. Andersen, *Solid State Commun.,* 1971, **9**, 1763.
20 G. Krier, O. K. Andersen and O. Jepsen, unpublished work.
21 R. Mauricot, P. Gressier, M. Evain and R. Brec, *J. Alloys Compd.,* 1995, **223**, 130.
22 R. D. Shannon, *Acta Crystallogr., Sect. A*, 1976, **32**, 751.
23 C. Rickel and R. Schöllhorn, *Mater. Res. Bull.,* 1975, **10**, 629.
24 G. Gauthier, S. Jobic, F. Boucher, P. Macaudière, R. Brec and J. Rouxel, *J. Mater. Chem.*, to be submitted.
25 R. Brec, G. Ouvrard, M. Evain, P. Grenouilleau and J. Rouxel, *J. Solid State Chem.,* 1983, **7**, 174.
26 E. I. Stiefel, R. Eisenberg, R. C. Rosenberg and H. B. Gray, *J. Am. Chem. Soc.,* 1966, **88**, 2956.
27 M. Evain, R. Brec and M. Whangbo, *J. Solid State Chem.,* 1987, **7**, 244.
28 H. P. Beck and C. Strobel, *Z. Anorg. Allg. Chem.,* 1986, **535**, 229.
29 A. Cade, M. Ribes, E. Philippot and M. Maurin, *C. R. Acad. Sci. Paris, Ser. C,* 1972, **274**, 1054.
30 (*a*) L. Beaury and P. Caro, *J. Phys. Fr.,* 1990, **51**, 471; (*b*) L. Beaury and P. Caro, *C. R. Acad. Sci. Paris, Ser. II,* 1993, **316**, 595.
31 P. Wu, Amy E. Christuk and J. A. Ibers, *J. Solid State Chem.,* 1994, **110**, 337.
32 A. C. Sutorik, J. Albritton-Thomas, C. R. Kannewurf and M. G. Kanatzidis, *J. Am. Chem. Soc.,* 1994, **116**, 7706.
33 (*a*) A. V. Prokoviev, A. I. Shelykh, A. V. Golubkov and I. A. Smirnov, *J. Alloys Compd.,* 1995, **219**, 172; (*b*) R. Mauricot, P. Gressier, M. Evain and R. Brec, *J. Alloys Compd.,* 1995, **223**, 130; (*c*) A. V. Prokoviev, A. I. Shelykh and B. T. Melekh, *J. Alloys Compd.,* 1996, **242**, 41; (*d*) C. Witz, D. Huguenin, J. Lafait, S. Dupont and M. L. Theye, *J. Appl. Phys.,* 1996, **79**, 1; (*e*) R. Mauricot, J. Dexpert-Ghys and M. Evain, *J. Lumin.,* 1996, **69**, 41; (*f*) M.-A. Perrin and E. Wimmer, *Phys. Rev. B,* 1996, **54**, 2428; (*g*) V. Zhukov, R. Mauricot, P. Gressier and M. Evain, *J. Solid State Chem.,* 1997, **128**, 197.
34 C. J. Bradley, A. P. Cracknell, in *The Mathematical Theory of Symmetry in Solids*, Clarendon, Oxford, 1972.
35 (*a*) S. Hufner and G. K. Wertheim, *Phys. Rev. B,* 1973, **7**, 5086; (*b*) M. Campagna, G. K. Wertheim and Y. Baer, in *Photoemission in Solids,* ed. L. Ley and M. Cardona, Springer-Verlag, Berlin, 1979,

p. 217; (*c*) J. K. Lang, Y. Baer and P. A. Cox, *Phys. Rev. Lett.,* 1979, **42**, 74; (*d*) F. Lopez-Aguilar and J. Costa-Quintana, *Phys. Status Solidi B,* 1983, **118**, 779.
36 (*a*) R. Mauricot, PhD Thesis, University of Nantes, 1995; (*b*) I. Mörke, E. Kaldis and P. Watcher, *J. Magn. Magn. Mater.,* 1985, **52**, 335.
37 G. Gauthier, S. Jobic, P. Macaudière, R. Brec and J. Rouxel, *J. Solid State Chem.*, to be submitted.

Paper 7/04702I; *Received* 3*rd July*, 1997